Global Modeling of Land Water and Energy Balances. Part I: The Land Dynamics (LaD) Model

P. C. D. MILLY

U.S. Geological Survey and NOAA/Geophysical Fluid Dynamics Laboratory, Princeton, New Jersey

A. B. SHMAKIN*

NOAA/Geophysical Fluid Dynamics Laboratory, Princeton, New Jersey

(Manuscript received 18 July 2001, in final form 9 January 2002)

ABSTRACT

A simple model of large-scale land (continental) water and energy balances is presented. The model is an extension of an earlier scheme with a record of successful application in climate modeling. The most important changes from the original model include 1) introduction of non-water-stressed stomatal control of transpiration, in order to correct a tendency toward excessive evaporation; 2) conversion from globally constant parameters (with the exception of vegetation-dependent snow-free surface albedo) to more complete vegetation and soil dependence of all parameters, in order to provide more realistic representation of geographic variations in water and energy balances and to enable model-based investigations of land-cover change; 3) introduction of soil sensible heat storage and transport, in order to move toward realistic diurnal-cycle modeling; 4) a groundwater (saturated-zone) storage reservoir, in order to provide more realistic temporal variability of runoff; and 5) a rudimentary runoff-routing scheme for delivery of runoff to the ocean, in order to provide realistic freshwater forcing of the ocean general circulation model component of a global climate model. The new model is tested with forcing from the International Satellite Land Surface Climatology Project Initiative I global dataset and a recently produced observation-based water-balance dataset for major river basins of the world. Model performance is evaluated by comparing computed and observed runoff ratios from many major river basins of the world. Special attention is given to distinguishing between two components of the apparent runoff ratio error: the part due to intrinsic model error and the part due to errors in the assumed precipitation forcing. The pattern of discrepancies between modeled and observed runoff ratios is consistent with results from a companion study of precipitation estimation errors. The new model is tuned by adjustment of a globally constant scale factor for non-water-stressed stomatal resistance. After tuning, significant overestimation of runoff is found in environments where an overall arid climate includes a brief but intense wet season. It is shown that this error may be explained by the neglect of upward soil water diffusion from below the root zone during the dry season. With the exception of such basins, and in the absence of precipitation errors, it is estimated that annual runoff ratios simulated by the model would have a root-mean-square error of about 0.05. The new model matches observations better than its predecessor, which has a negative runoff bias and greater scatter.

1. Introduction

A healthy balance among observation, theory, and modeling is the key to development of better description, understanding and prediction of the global water cycle and its connection with the global climate system (U.S. National Research Council 1990, 1998; Milly and Dunne 2002a, manuscript submitted to *Water Resour. Res.*, hereafter MIDUa). Models are a critical component of this balance, because they serve as an objective and quantitative framework for the statement and testing of scientific hypotheses and for the evaluation of the state of scientific progress. Additionally, models often provide the link between theory and application; models, when they embody reasonable mathematical summaries of relevant scientific understanding, allow use of that understanding in the description and prediction of hydrologic and related environmental processes.

In research on climate dynamics and global hydrology, one of the earliest and most productive models of land (continental) water and energy balance has been that of Manabe (1969). In this model, sensible heat capacity of land is ignored. Liquid water capacity of each land cell is lumped into a single soil water reservoir. Evaporation is proportional to the vapor pressure gra-

* Current affiliation: Institute of Geography, Russian Academy of Sciences, Moscow, Russia.

Corresponding author address: Dr. P. C. D. Milly, Water Resources Division, U.S. Geological Survey, NOAA/Geophysical Fluid Dynamics Laboratory, P.O. Box 308, Princeton, NJ 08542.
E-mail: cmilly@usgs.gov

dient in the atmospheric surface layer, with surface control acting only when soil water is limited and snow is absent. Runoff is produced only when precipitation (or snowmelt) input to the soil would otherwise cause exceedance of a prescribed soil water capacity. The simplicity of this model and its realistic constraints on water and energy balances have allowed it to be used effectively in a series of benchmark studies on global climate (e.g., Manabe 1969), climate variability (e.g., Delworth and Manabe 1989), and climate change (e.g., Haywood et al. 1997).

a. Rationale for further model development

For increased realism and detail, but especially in order to permit analyses of new scientific problems, the model of Manabe (1969) may benefit from inclusion of additional physical processes. One prominent feature of the model is the aforementioned lack of surface control of evaporation when water is freely available, which is inconsistent with the recognized reality of stomatal control in the absence of water stress. In stand-alone intercomparison of land models (i.e., numerical experiments run with prescribed atmospheric and radiative forcing), non-water-stressed stomatal control of transpiration has been shown to be a major factor explaining the intermodel differences of long-term water balance (Chen et al. 1997). Furthermore, stomatal control of continental water balance may be a crucial factor in the global hydrospheric response to greenhouse warming (Henderson-Sellers et al. 1995; Sellers et al. 1996a).

Another major simplifying assumption in the model of Manabe (1969) is the neglect of sensible heat storage by land. Ground storage of heat is a very small term in the daily mean energy balance but can be a large term at subdaily timescale. In the numerical experiments within which Manabe's (1969) model has been used, neglect of heat storage has been well justified by the absence of a diurnal cycle of insolation. In the future, with increased attention to finer-scale realism in climate modeling, we anticipate increasing needs for inclusion of realistic diurnal forcing in the climate model. Over many land types, realistic simulation of the energy balance then will require recognition of sensible heat storage by soil and/or vegetation.

Groundwater storage (i.e., storage in the saturated zone below the water table) must be quantified in order to produce realistic time series of river discharge from model runoff fields (Lohmann et al. 1996; Milly and Wetherald 2002, manuscript submitted to *Water Resour. Res.,* hereafter MIWE). Discharge time series are useful for model evaluation and for climate change impact studies. Of course, any model of river discharge requires also the delineation of drainage basins of the world in order to define the areas over which runoff is collected to form the flow of a given river.

The model of Manabe (1969) used globally constant values for all surface parameters except snow-free surface albedo, whose distribution was tied to the global vegetation distribution. Since the work of Dickinson et al. (1981) and Sellers et al. (1986), it has become accepted practice among climate modelers to allow all surface parameters to vary globally (and seasonally) as functions mainly of given vegetation and soil characteristics. Underlying this practice is an assumption that the characteristics and the functional dependencies are sufficiently well known to make this be an improvement over global constants. Clearly, such dependencies are needed in models if the hydroclimatic consequences of land-cover changes are to be estimated by use of models. In Parts II (Milly and Shmakin 2002) and III (Shmakin et al. 2002) of this series of papers, we will explore the increase in model performance that results from introduction of such dependencies into our model.

This work has benefited greatly from many papers in this field during the last two decades and from the authors' participation in the Project for Intercomparison of Land–Surface Parameterization Schemes (Henderson-Sellers et al. 1993). None of the model developments discussed above is entirely original and many other developments that have been advanced in other models are not addressed here. The intended contribution of this paper is in the particular combination of certain modeling ideas and, especially, in the application of error-characterized observational data to model evaluation. We have chosen to focus on those model aspects that seem to be the most important for the next step in the evolutionary development of the land model first formulated by Manabe (1969).

b. Model evaluation with uncertain observational data

MIDUa concluded that the weak link in large-scale hydrologic research is the use of observational data as a constraint on theory and model development. Recent years have seen a proliferation of dynamic models of the water and energy balances of the global landmasses. Most models are used in a coupled mode with atmospheric and oceanic models to simulate climate and to predict weather. Other models are used in stand-alone mode, often regionally, to support investigations of biogeochemical cycling. Testing of these global land models with observations is a challenging exercise, because suitable datasets are generally not available. Models typically require input of several atmospheric forcing variables (precipitation, radiation, wind speed, air humidity, and air temperature) at high temporal (minutes to an hour) and spatial (order of 100 km) resolution. At the same time, independent observational data on water and/or energy fluxes are required for model evaluation.

Most model evaluation efforts have focused on testing models with observational data mainly from a single site (Chen et al. 1997) or a small area (Schlosser et al.

2000). If one is willing to work without detailed knowledge of the land forcing, then greater spatial scope of investigations is possible, and new ways arise to use observations. Lohmann et al. (1998) evaluated a large collection of models using river discharge and atmospheric vapor budget data from the Red-Arkansas river basins, and Costa and Foley (1997) compared a model to observations over the Amazon basin. Levis et al. (1996) and investigators in the Global Soil Wetness Project (e.g., Zhang et al. 1999; Oki et al. 1999) have presented model evaluations of global scope.

Optimal use of observational data in assessments of model performance requires an understanding of uncertainties in the data (MIDUa). Accuracy increases the power of the data to detect model errors, and failure to recognize the presence of data inaccuracy leads potentially to inflated estimates of model errors. One approach to control of errors in forcing is to screen out data judged to have unacceptable errors. Of course, this requires that some error measure be defined and evaluated, and that some threshhold value for acceptance be set. The most efficient screening criteria will filter out data with unacceptable errors (which could be mistaken for model errors) and will accept data with sufficiently small errors (in order to maximize the power of the evaluation dataset). As an indirect measure of data error, Oki et al. (1999) adopted a critical rain gauge density criterion in their analysis. Quantitative a priori estimates of uncertainty in datasets (e.g., MIDUa) should be helpful in the formulation of efficient screening criteria. An alternative approach is to weight the observations according to data uncertainty. We use a combination of these approaches in this study.

c. Objectives

The objectives of this paper are 1) to describe the Land Dynamics (LaD) model, which is a revised version of Manabe's (1969) model of land water and energy balances at large scales, 2) to illustrate an approach for land model evaluation in the presence of precipitation uncertainty, and 3) to evaluate the performance of the LaD model by comparison with observations. In the process, opportunities also arise to test the precipitation error estimates of MIDUa, and to explore the role of soil physics in interseasonal water storage below the root zone.

2. Model description

a. Conceptualization of water and energy storage

The domain to be modeled is divided into nonoverlapping cells, and the water and energy balance of each cell is treated separately. A cell may be either glaciated or nonglaciated. Glacier dynamics are not treated, and a glacier cell is assumed to be permanently glaciated, although net losses of glacier ice by melting and sublimation are allowed.

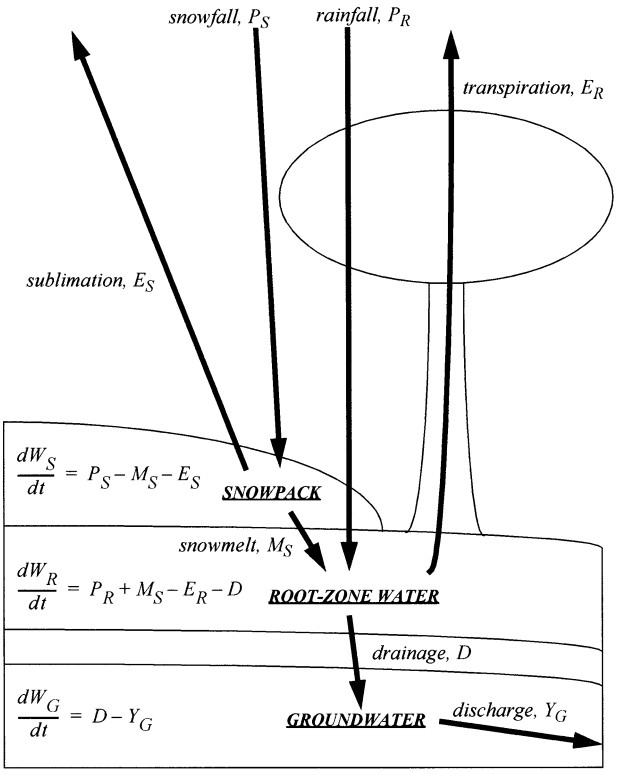

FIG. 1. Water fluxes and stores in the LaD model.

Total water storage (W, mass of water per unit horizontal area) within each nonglaciated cell is composed of a snowpack store (W_S), a root-zone store (W_R), and a groundwater (W_G) store (Fig. 1). Glaciated cells have only the snowpack store and a glacier-ice store W_I. In general, we may write

$$W = W_S + W_R + W_G + W_I, \tag{1}$$

with the understanding that one or more of these terms is always zero. Intercepted water is not considered in the model. Liquid water content of the snowpack is assumed to be small at all times. The mass W_R of water is assumed to be contained in a root zone defined between the land surface and an effective depth of rooting, Z_R. Following convention in climate modeling, W_R is defined as the amount of water in excess of ''dead storage'' associated with the assumed wilting point of the dominant vegetation type. At some depth greater than Z_R is a dynamic water table; storage in the saturated zone below the water table is given by W_G. Both W_R and W_G are assumed to remain in the liquid state, regardless of temperature; subsurface phase change is not allowed. The possibility of a constant storage of water (e.g., at field capacity) between the root zone and the water table is allowed, but this unchanging amount does not enter the balance equations. Water in the glacier ice store is all frozen.

Total energy storage (S) (heat energy per unit horizontal area) is equal to the sum of latent heat of fusion

of the snowpack (S_S) and the glacier (S_I) and sensible heat content of the ground (S_R),

$$S = S_S + S_I + S_R. \tag{2}$$

Sensible heat storage, represented by a one-dimensional temperature distribution $T(z)$, is allowed in the soil or ice sheet and in snowpack, if present. For simplicity, however, several approximations are made. Evolution of $T(z)$ obeys a simple heat conduction equation. The heat capacity of any aboveground vegetation is neglected, and its temperature is taken to be the same as that of the ground surface; the latter assumption will tend to cause an overestimate of ground heat storage at the diurnal timescale because of excessive atmosphere-ground coupling. The moving surface boundary and temporal changes in heat capacity and thermal conductivity associated with snowpack dynamics are ignored. Likewise, temporal changes in thermal properties caused by changes in soil water content are ignored; effectively, changes in heat capacity and thermal conductivity of soil caused by changes in soil water content are neglected. Soil water is not allowed to freeze, so no latent heating terms appear in the subsurface. Snowmelt occurs only at the upper surface of any snowpack or exposed glacier ice. Any meltwater flows instantaneously to the bottom of the snowpack, whose liquid retention capacity is neglected.

The heat contents of the snowpack and the glacier are given by

$$S_S = -L_f W_S, \tag{3}$$

$$S_I = -L_f W_I, \tag{4}$$

where L_f is the latent heat of fusion of water, and sensible heat storage is given by

$$S_R = C \int_0^\infty T \, dz, \tag{5}$$

where C is volumetric heat capacity.

b. Water-balance equations

Snowpack water balance is given by

$$\frac{dW_S}{dt} = P_S - M_S - E_S, \tag{6}$$

where P_S is the rate of frozen precipitation, M_S is the rate of melting of snowpack, and E_S is the rate of sublimation from the snowpack. For nonglaciated cells, snowmelt and rainfall (P_R) feed the root-zone store, which is depleted by evaporation (E_R) and root-zone drainage (D),

$$\frac{dW_R}{dt} = P_R + M_S - E_R - D. \tag{7}$$

Drainage from the root zone replenishes the groundwater store, which, in turn, yields discharge (Y_G) to the surface water network,

$$\frac{dW_G}{dt} = D - Y_G. \tag{8}$$

For glaciated cells, (6) applies to snowpack evolution, and W_R and W_G are permanently zero. Glacier ice is depleted by sublimation (E_I) and melt (M_I),

$$\frac{dW_I}{dt} = -E_I - M_I. \tag{9}$$

Any meltwater from overlying snowpack (M_S) and any rainfall immediately combine with M_I as discharge from the glacier to the surface water network, Y_I,

$$Y_I = P_R + M_S + M_I. \tag{10}$$

The overall cell water balance can be obtained for unglaciated cells by summation of (6), (7), and (8), and for glaciated cells by summation of (6) and (9). The result may be written in general as

$$\frac{dW}{dt} = P - E - Y, \tag{11}$$

where P is precipitation (sum of P_R and P_S), E is rate of vapor transfer from ground to atmosphere (E_S if snowpack is present, E_R for snowfree nonglaciated cell, E_I for snow-free glaciated cell), and Y is rate of water supply to the surface water network (Y_G for nonglaciated cell, and Y_I for glaciated cell).

c. Energy-balance equations

The simple energy-balance equation for snowpack is obtained from (3) and (6),

$$\frac{dS_S}{dt} = L_f(M_S + E_S - P_S), \tag{12}$$

and for glacier ice from (4) and (9),

$$\frac{dS_I}{dt} = L_f(M_I + E_I). \tag{13}$$

The energy balance of the ground may be written most simply as

$$\frac{dS_R}{dt} = G, \tag{14}$$

where G is the sensible heat flux into the ground. The sensible heating of the ground is determined through surface energy balance with radiation, latent and sensible heating of the atmosphere, and phase change of glacier ice or snow,

$$G = R_n - LE - H - L_f M - L_f(E_S + E_I), \tag{15}$$

where R_n is net heating of the land by radiant energy transfer with the atmosphere, L is the latent heat of vaporization of water, H is the rate of sensible heat flux from land to atmosphere, and M is the melt rate

(sum of M_S and M_I). Finally, an overall energy balance, applicable for either glaciated or unglaciated cells, is found by summation of (12), (13), and (14), together with (15),

$$\frac{dS}{dt} = R_n - LE - H - L_f P_S. \tag{16}$$

Temperature below the surface is tracked by a heat conduction equation,

$$C\frac{\partial T}{\partial t} = -\frac{\partial q_h}{\partial z}, \tag{17}$$

where q_h is the vertical flux of heat,

$$q_h = -\lambda\frac{\partial T}{\partial z}, \tag{18}$$

where λ is thermal conductivity. Boundary conditions on (18) are

$$q_h = 0, \qquad z \to \infty, \tag{19}$$

$$q_h = G, \qquad z = 0. \tag{20}$$

d. Additional flux equations

The balance equations (6), (7), (8), (9), (12), (13), and (17) can be solved only when additional expressions are provided for various water fluxes (vapor fluxes E_S, E_R, E_I; root-zone drainage rate D; groundwater discharge rate Y_G; melt rates M_S, M_I) and energy fluxes (net radiation R_n; sensible heat flux to atmosphere H). Computation of these terms is summarized here.

The land model may be run either in stand-alone mode or coupled to an atmospheric model. In stand-alone mode, forcing consists of the near-surface atmospheric state and downwelling radiative fluxes, and the surface fluxes are computed as functions of these forcing variables and the surface states. In coupled mode, the same is true, but the surface fluxes feed back to the atmospheric state through the atmospheric model. In either case, we may write

$$H = \frac{\rho_a c_p}{r_a}(\theta_o - \theta_a), \tag{21}$$

where r_a is the aerodynamic resistance for scalar transfer, θ_o and θ_a are potential temperature at the surface and at some given level z_a in the atmospheric surface layer, ρ_a is the density of air, and c_p is specific heat of air at constant pressure. For the model applications described here, the aerodynamic resistance r_a is dependent on momentum and scalar roughness lengths (z_o and z_T), on the height z_a at which θ_a is defined, and on the Monin–Obukhov length L_{MO}, which is a measure of atmospheric stability,

$$r_a = r_a(z_0/L_{\mathrm{MO}}, z_T/L_{\mathrm{MO}}, z_a/L_{\mathrm{MO}}). \tag{22}$$

Our implementation of (22) is essentially that described by Garratt (1992). Under stable conditions, however, we use the similarity function $\Phi(x) = 1 + x(5 + x/2)/(1 + x)$, instead of the more conventional $\Phi(x) = 1 + 5x$, in order to avoid excessive suppression of vertical exchange (I. M. Held 2001, personal communication). We eliminate z_T by use of (Brutsaert 1982, 103–110; Garratt 1992, p. 93)

$$\ln(z_o/z_T) = 2. \tag{23}$$

Vapor fluxes from glacier or snow surfaces are similarly parameterized as

$$E_{I,S} = \frac{\rho_a}{r_a}[q_s(T_o) - q_a], \tag{24}$$

where $q_s(T_o)$ is the mixing ratio of water vapor associated with saturated conditions at the surface temperature and q_a is the mixing ratio at level z_a. When a snowpack is present, it covers the surface, so (24) describes sublimation from snowpack when the pack is present, and directly from the glacier ice otherwise.

When an unglaciated cell has no snowpack, the evaporation is given by a modified version of (24),

$$E_R = \frac{\rho_a}{(r_a + r_s)}[q_s(T_o) - q_a]\min\left[\left(\frac{W_R}{0.75W_R^*}\right), 1\right], \tag{25}$$

where r_s is a bulk stomatal resistance under conditions of negligible water stress and W_R^* is the maximum possible value of W_R. The final factor in (25) accounts for limitation of E_R by water stress. Milly (1992) has argued that the form of (25) (ignoring for the moment the new r_s term) is inconsistent with the empirical work upon which it is based and has suggested a modified formulation. That formulation, in essence, changes only the shape of the water stress function, but not its limiting behaviors, and subsequent sensitivity studies have shown little effect of this modification. Hence, for simplicity and for consistency with Manabe (1969), the form of (25) is retained here.

Root-zone drainage is assigned whatever value is needed to prevent root-zone water storage from exceeding a specified maximum value (field capacity), W_R^*,

$$D = \begin{bmatrix} P_R + M_S - E_R & \text{when } (P_R + M_S - E_R > 0) \quad \text{and} \quad (W_R = W_R^*) \\ 0 & \text{when } (P_R + M_S - E_R \le 0) \quad \text{or} \quad (W_R < W_R^*) \end{bmatrix}. \tag{26}$$

Efflux from groundwater storage is made proportional to storage (MIWE),

$$Y_G = W_G/\tau, \tag{27}$$

where the groundwater residence time τ is another model parameter. Our extremely simple runoff scheme assumes instantaneous downstream flow of all runoff ($Y_I + Y_G$). Equivalently, surface water storage is neglected. Thus, the discharge past any point on a river, at any time, is found as the summation over all upstream cells of the product of runoff rate and cell area at that time.

The snowmelt (or glacier melt) rate is whatever is necessary to prevent the surface temperature of the snowpack (or exposed glacier) from exceeding the freezing point. In practice, the energy balance is first solved under the assumption that no frozen water melts. If this would cause surface temperature to rise above freezing, then the temperature is set to freezing and melt is computed as the energy residual (Manabe 1969).

Net radiation, R_n, is computed as

$$R_n = R_s(1 - A) + R_l - \sigma T_o^4, \tag{28}$$

where R_s is downward solar radiation flux, A is surface albedo, R_l is atmospheric radiation, and σ is the Stefan–Boltzmann constant. Surface emissivity is taken to be unity. Albedo is taken as a weighted mean of snowfree albedo A_n (a surface parameter) and deep-snow albedo A_s,

$$A = (1 - \beta)A_n + \beta A_s, \tag{29}$$

where (Koster and Suarez 1996)

$$\beta = W_S/(W_S + W_S^*). \tag{30}$$

The snow-masking depth W_S^* is another surface parameter. Qualitatively, it accounts for the fact that the albedo of a surface generally increases with snow depth as more fractional area becomes snow covered and less vegetation and fewer surface features protrude from the snow. Snow albedo is given as a function of surface temperature, ranging from 0.45 to 0.6 over nonglaciated cells, and from 0.65 to 0.8 over glaciated cells.

e. Numerical discretization

General features of temporal and spatial discretization are outlined here. Specific choices for layer thicknesses, time step durations, and so forth, are not intrinsic to the model. Values used in this study are given later in the description of the experiments.

The ground temperature distribution $T(z)$ is represented by a series T_i with i from 1 to N, representing temperatures in successively deep layers of thickness Δ_i. Equations (17) and (18) are discretized accordingly. Condition (19) is replaced by a no-flux condition at the bottom of layer N. Condition (20) is applied by equating G to the flux into the top of the uppermost layer. The temperature T_1 of the uppermost layer is equated to the surface temperature T_o at all times.

The energy balance equations are integrated in time by finite differencing, with a fully implicit (backward difference) formulation. This formulation includes linear expansion of all surface flux terms with respect to surface temperature. This approach is chosen for its unconditional stability. In contrast with the usual numerical implementation of the model of Manabe (1969), no iteration on the nonlinearity is performed.

Given the energy-balance solutions, water balance equations for W_R, W_S, and W_I are solved explicitly (forward difference) with the same time step duration, with allowance for the possibility of complete emptying or saturation of stores during the course of the time step. Subsequently, (8) and (27) are integrated exactly for W_G, with a longer time step than for the primary water and energy balance solutions, and with time-average values of D.

f. Assignment of model parameters

The relations presented above contain a series of parameters that characterize the land. These are maximum root-zone soil water (W_R^*), bulk heat capacity of the ground (C), thermal conductivity of the ground (λ), surface roughness length (z_o), non-water-stressed bulk stomatal resistance (r_s), groundwater residence time (τ), snowfree surface albedo (A_n), and snow masking depth (W_S^*). All of these parameters are treated as constant over time. Most are assumed to vary from cell to cell as a function of cell vegetation type and cell soil type.

Vegetation type is defined using a classification very similar to that of Sellers et al. (1996b). A global map of vegetation type, at 1° resolution, is formed by grouping the 32 vegetation types of Matthews (1983) into a reduced set of 10 types (Table 1). Because one of these 10 model types is agricultural, and because we consider at this point only natural vegetation, only 9 types are actually present in the model's default vegetation map (Fig. 2). Soil type is defined on the basis of Zobler's (1986) global classification of near-surface (0–0.3 m) soil texture, which we take as a reasonable index of root-zone soil texture. Each cell covered by mineral soils is classified either as being dominated by coarse, medium, or fine soil, or as an areal mixture of two types or of all three types (Fig. 3, Table 2). A small fraction of the cells is classified as peat soils.

Values of A_n, z_o, and r_s are assigned (Table 1) mainly by use of results from Dorman and Sellers (1989). Seasonal cycles of each parameter were averaged over the year, with more weight given to seasons of higher water and energy fluxes, to obtain constant values. For r_s, the values so derived then were increased to account, in an average way, for environmental stresses, other than water limitation, that were excluded from the computations of Dorman and Sellers (1989); these stresses are associated with suboptimal values of atmospheric water vapor pressure deficit and leaf temperature. The r_s values were increased by a factor of 2 for the tall (first five)

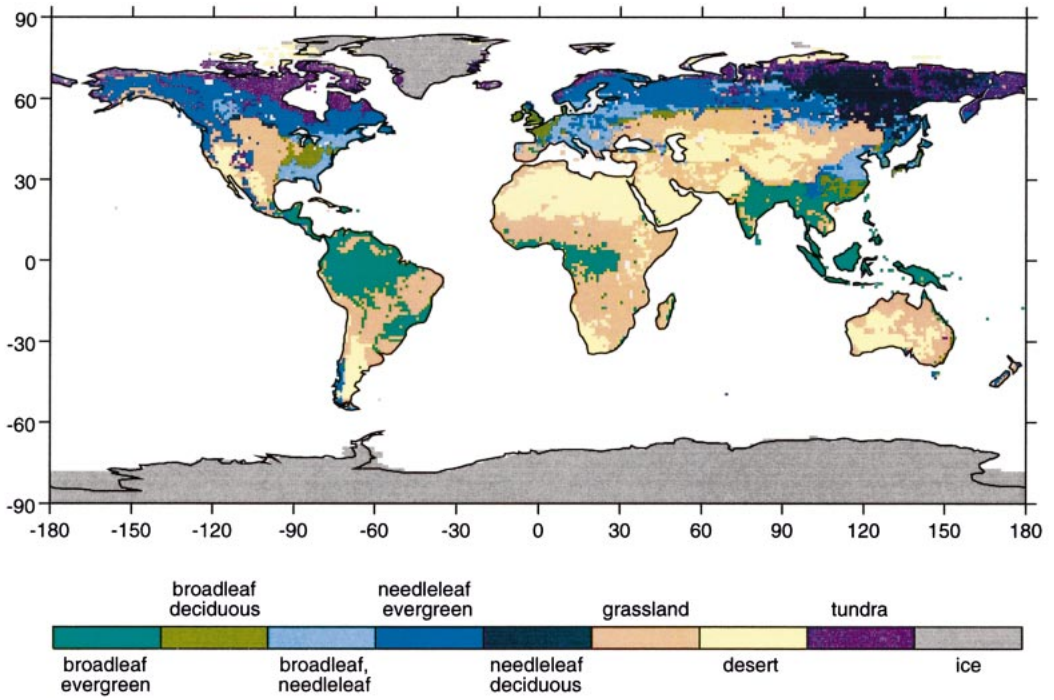

FIG. 2. Global distribution of natural vegetation type in the LaD model.

vegetation types and by a factor of 1.3 for short vegetation, on the basis of the review of the subject by Dorman and Sellers (1989). The snow-masking depth was subjectively assigned values of 100 kg m^{-2} for tall vegetation and 40 kg m^{-2} otherwise, corresponding to light, unpacked snow depths of 1 m and 0.4 m, respectively.

The root-zone water capacity (W_R^*) is taken as the product of available water capacity of soil (AWC, Table 2) and an effective rooting depth of vegetation Z_R, following the general approach of Dunne and Willmott (1996). Available water capacities of coarse, medium, and fine soils and of peat soil are taken from Dunne and Willmott. Values for mixtures of mineral soils are averages of the primary values. To derive an effective rooting depth, we assume the root biomass density R to vary with depth according to

$$R(z) = R_o e^{-z/\zeta}, \tag{31}$$

where R_o is the root biomass density at the surface and ζ is an extinction depth scale. We defined the effective depth of the root zone as that depth at which the root biomass decays to some critical value R_c,

$$Z_R = \zeta \ln(R_o/R_c). \tag{32}$$

The critical root biomass is assumed to be a global constant, which we set at 0.5 kg m^{-3}; this value was chosen to give typical forest rooting depths of about 1 m. Our framework for estimation of Z_R is arbitrary, but seems to be at least as rational as any available alternatives. Values of both R_o and ζ were computed from biome-based summaries of rooting properties provided by Jackson et al. (1996), yielding the rooting depth values shown in Table 1. The very small value obtained

TABLE 1. Vegetation types and associated characteristics. Matthews's type B was split between two of our types: the region of larch forest in northeast Asia was placed in our type 5 (needleleaf deciduous), and the remainder was placed in our type 2 (broadleaf deciduous).

Type index	Vegetation type	Matthews's types	A_n	z_o (m)	r_s (sm^{-1})	Z_R (m)	W^*_S (kg m^{-2})
1	Broadleaf evergreen	1, 2, 3, 9	0.13	2.65	100	0.9	100
2	Broadleaf deciduous	5, B (see caption)	0.13	0.90	300	1.0	100
3	Broadleaf, needleleaf	A	0.12	1.20	200	1.1	100
4	Needleleaf evergreen	4, 7, 8, E	0.11	0.90	160	0.6	100
5	Needleleaf deciduous	B (see caption), G	0.13	0.80	500	0.6	100
6	Grassland	6, C, D, F, N–T	0.20	0.07	130	0.6	40
7	Desert	H, J, L, U	0.32	0.01	0	1.0	40
8	Tundra	I, K, M	0.16	0.07	390	0.3	40
9	Agriculture	W	0.16	0.40	130	0.04	40
10	Ice	V	0.65	0.01	—	—	40

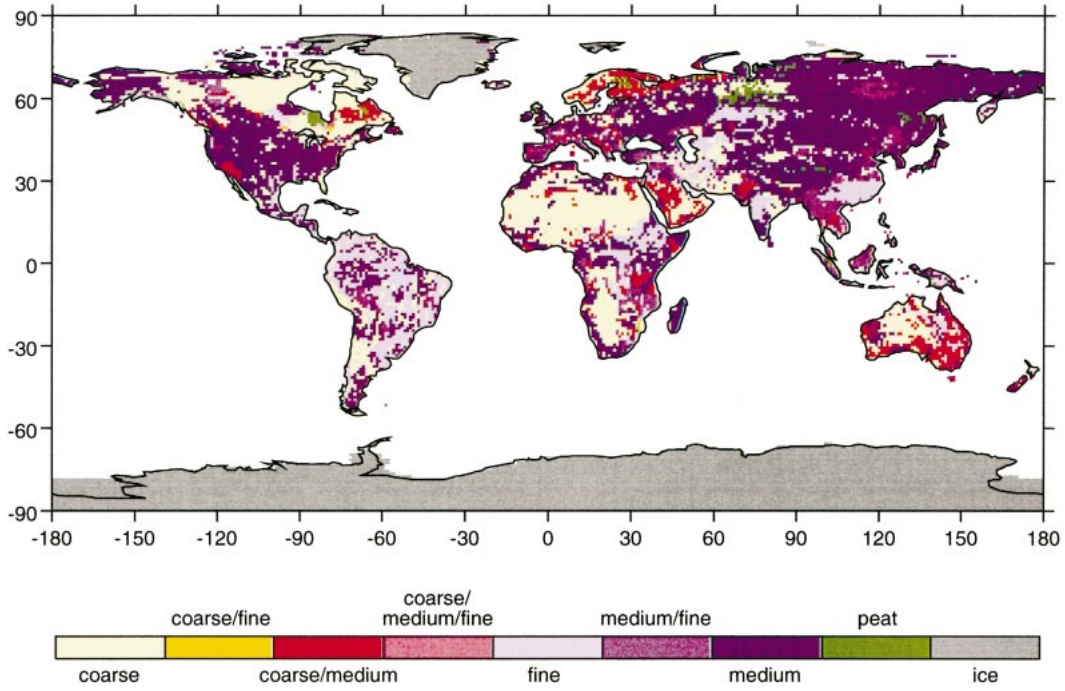

FIG. 3. Global distribution of soil type in the LaD model. (Mineral soils are classified by near-surface texture, with the order in the legend determined by values of available water content, which has a minimum value in coarse soils and a maximum value in medium soils.)

for agriculture probably reflects invalidity of using a single value of R_c for both natural and agricultural vegetation. The questionable value for agricultural land presents no problem in the present application, because natural vegetation distributions are used.

The rules given above for determining r_s and Z_R were not followed for the desert vegetation type, because vegetation is very sparse in a desert environment, whereas our formulation of evaporative loss from the root zone, given in (25), effectively assumes full vegetation cover. The use of an r_s typical of desert vegetation to describe overall surface resistance would suppress total evaporation unnaturally, ignoring the direct pathway of evaporation from bare soil. Because plant transpiration is not necessarily the dominant pathway for evaporative water loss, the use of rooting depth to characterize water storage capacity also is questionable. In view of these considerations, we arbitrarily assign desert values of 0 and 1 m to r_s and Z_R, respectively. These values are sufficient to guarantee that desert cells will retain nearly all precipitation and return it to the atmosphere. In our applications, any errors in water-balance partitioning and its timing would appear to be insignificant.

TABLE 2. Soil types and associated characteristics.

Type index	Soil type	AWC (kg m^{-3})	C (J m^{-3} K^{-1})	λ/C (m^2 s^{-1})
1	Coarse	63	1.8×10^6	8.3×10^{-7}
2	Medium	132	2.0×10^6	4.0×10^{-7}
3	Fine	109	2.6×10^6	5.2×10^{-7}
4	Coarse/medium	98	1.9×10^6	6.2×10^{-7}
5	Coarse/fine	86	2.2×10^6	6.8×10^{-7}
6	Medium/fine	120	2.3×10^6	4.6×10^{-7}
7	Coarse/medium/fine	101	2.1×10^6	5.8×10^{-7}
8	Peat	445	3.0×10^6	1.3×10^{-7}
9	Ice	—	1.6×10^6	1.1×10^{-6}

Ground heat capacity (C) and thermal conductivity (λ) are assigned as functions of soil type, regardless of the possible presence of snowpack (Table 2). The values are based on various published values for sands (coarse), silt loam (medium), clay (fine), and peat, at typical levels of saturation.

MIWE estimated the values of the basin residence time (τ) for the basins in the dataset of MIDUa. The values of Milly and Wetherald for a given basin are assigned to all cells within the basin. Where two basins contained the same cell (because of nesting of some basins), one of the two basins was excluded from the entire analysis. For all cells outside of basins in the dataset, τ is assigned a value of 30 days; all results presented here, however, are for basins in which τ was available from MIDUa.

g. Recovery of Manabe (1969) model

It is possible to reduce the model described above to one that is very close to that of Manabe (1969). The following reductions are needed:

1) Set non-water-stressed stomatal resistance r_s to zero, eliminating stomatal control of evaporation.

2) Set C to zero, eliminating heat storage S_R in the ground.
3) Set groundwater residence time τ to zero, eliminating groundwater storage W_G.
4) Use globally constant values of 150 kg m^{-3} for the available water capacity and 1 m for rooting depth (or any other values whose product is 150 kg m^{-2}).
5) Use a globally constant value of 0.01 m for the surface roughness length.
6) Assume similarity of interfacial transfer processes for momentum, heat and vapor, instead of (23).
7) Use the albedo distribution of Manabe (1969), rather than that implied by Table 1.

3. Model evaluation

a. Experiments

We used the International Satellite Land Surface Climatology Project (ISLSCP) Initiative I dataset (Meeson et al. 1995) as the primary source of forcing for the land model. The ISLSCP dataset contains downward shortwave and longwave radiation, total precipitation, surface pressure, and near-surface atmospheric temperature, humidity, and wind speed, on a global 1° grid, every 6 h for calendar years 1987 and 1988. These variables are based on a variety of observations, models, and analyses. We specified precipitation as rain when near-surface air temperature was above the freezing point and snow otherwise.

The consideration of precipitation uncertainty is a crucial need in land water-balance model evaluation, but ISLSCP precipitation data have unknown error characteristics. MIDUa, however, have developed error-characterized estimates of monthly basin precipitation for 175 large (median area of 51 000 km^2) basins worldwide. To allow use of the latter error estimates, together with the high temporal resolution of ISLSCP, we merged the basin precipitation estimates into the ISLSCP dataset. We adjusted the 6-hourly ISLSCP precipitation data so that they would agree with the monthly, basin-mean values determined by MIDUa. A scale factor was computed as the ratio of Milly and Dunne's monthly, basin-mean value to that implied by ISLSCP; then the 6-hourly ISLSCP precipitation values for all gridpoints located within any basin were scaled by the factor for that month and basin. No nested basins were used, so any grid cell could fall in at most one basin, allowing unique definition of the scale factor.

Incoming shortwave and longwave radiation similarly were scaled to match the data in the NASA Langley Surface Radiation Budget data set. This scaling was done in order to use a more recent, and presumably more accurate, estimate of the radiative fluxes and to provide consistency with the analysis of MIDUa.

This paper describes the results of five numerical experiments summarized below.

1) NEW Used the new land model with all parameter specifications as described above.
2) TUNED Same as NEW but with global scale factor of 0.4 applied to r_s.
3) OLD Used the model to mimic the Manabe (1969) model.
4) RS0 Same as NEW but with $r_s = 0$ globally.
5) RS0Z01 Same as NEW but with $r_s = 0$ and $z_o = z_T = 0.01$ m globally.

The first two of these are an initial test experiment and a calibration experiment. The other three experiments illuminate the difference in behavior between this model and that of Manabe (1969).

Aside from the distinctions noted above, all experiments were run under identical conditions. All water stores were initialized at zero storage. All temperature stores were initialized at 260 K (not relevant for OLD, which has negligible heat capacity). The 6-hourly forcing was interpolated linearly to hourly forcing. The effective height of atmospheric forcing (z_a) was taken to be 10 m; two additional sensitivity experiments indicated that the results of NEW were highly insensitive to a fourfold increase or decrease of this value of z_a. The energy, soil water, and snowpack equations were solved with an hourly time step, and the groundwater equation was solved with a 1-day time step. The number of soil layers was taken to be 5, with thicknesses Δ_i of 0.005, 0.045, 0.10, 0.35, and 1.0 m. The model was run from the start of 1987 through 1988. Additional experiments indicated that the 1988 results were insensitive to initial conditions at the start of 1987; that is, that one year of spinup was sufficient for these experiments.

b. Observations and precipitation uncertainty

The basin data of MIDUa were used for the comparisons with observations. Only 104 of Milly and Dunne's 175 basin discharge time series include data for all of 1988. Of these, several more were eliminated to avoid nesting, so that the precipitation adjustments could be uniquely defined. Two more were eliminated because a significant fraction of their areas did not have forcing values on the ISLSCP CD-ROM, because of large lakes in the basin. Several more were excluded because they had fewer than five gauges, preventing application of the error estimates developed by MIDUa. Together, these requirements resulted in a total of 82 basins with the necessary discharge data, precipitation data, and precipitation error characteristics.

The model was evaluated primarily by comparison with river discharge observations for 1988, following a 1-yr (1987) spinup period. To quantify model performance, we compared modeled and observationally determined 1988 runoff ratios (basin discharge divided by basin precipitation volume); to obtain the model discharge, we used basin averages of Y_G. Rather than runoff ratios, runoff volumes or average runoff depths (volume

per unit basin area) could have been used, but either of these would have created an excessive range of values across basins, hindering an overall assessment of error. Also, rather than normalizing by precipitation, we could have normalized by observed runoff. We felt that this would place undue weight upon minute errors in runoff from arid basins, which are perhaps the least important for the climatic applications of interest.

Let p be the basin-mean, annual-total precipitation in any basin during 1988, and let $\hat{p}$ be the estimate of p derived from observations by MIDUa. The estimation error of annual precipitation, denoted by ε, is given by

$$\varepsilon = \hat{p} - p. \tag{33}$$

MIDUa separated this total error for any particular year n into two parts,

$$\varepsilon = \varepsilon_a + \varepsilon_n, \tag{34}$$

where ε_a is the error in the estimate $\hat{p}_a$ of the long-term, annual-mean precipitation, and ε_n is the error in the estimate of the precipitation anomaly for year n. Statistical behavior of ε_a was characterized by a parameter ψ_a,

$$\psi_a = [E\{\varepsilon_a^2\}]^{1/2}/\hat{p}_a, \tag{35}$$

where $E\{\ \}$ is the expectation operator. Components of ε_a considered include expected spatial-sampling errors in the absence of orographic effects, spatial-sampling errors associated with orographic effects, and errors in adjustments for gauge bias. MIDUa also applied standard correlation-based methods to develop estimates of the variance σ_n^2 of the anomaly errors ε_n. Herein we assume independence of ε_a and ε_n to obtain a measure of the total estimation error in basin-mean precipitation,

$$E\{\varepsilon^2\} = (\psi_a \hat{p}_a)^2 + \sigma_n^2. \tag{36}$$

c. Effect of precipitation input error on model runoff

The precipitation error ε will contribute to a discrepancy between modeled and observed runoff ratios. Here we develop an estimate of that contribution. Let $\hat{\delta}$ be the apparent runoff ratio error of the model for a given basin,

$$\hat{\delta} = \frac{y_m(\hat{p}) - \hat{y}}{\hat{p}}, \tag{37}$$

where y_m is the modeled basin-mean, annual total (1988) discharge (which depends on the value $\hat{p}$ used to run the model, among other variables), and $\hat{y}$ is the observed discharge. The apparent error is decomposed as

$$\hat{\delta} = \delta + \delta^*, \tag{38}$$

where δ is defined as the error that would have been found if the model had been run with the correct precipitation, p,

$$\delta = \frac{y_m(p) - \hat{y}}{p}, \tag{39}$$

and δ^* is the component of the apparent error due to error in the precipitation forcing. As an approximation, we assume that model runoff can be linearized locally in annual precipitation (MIDUb),

$$y_m(p) = y_m(\hat{p}) + \frac{dy}{dp}(p - \hat{p}), \tag{40}$$

where dy/dp is constant for a given basin. We can then derive an expression for δ^*,

$$\delta^* = \left(\hat{\delta} - \frac{dy}{dp}\right)\frac{(p - \hat{p})}{p}. \tag{41}$$

Ignoring the difference between $\hat{p}_a$ and the p in the denominator, and using (33), we obtain

$$\delta^* = \left(\hat{\delta} - \frac{dy}{dp}\right)(\varepsilon/\hat{p}_a). \tag{42}$$

The $\hat{\delta}$ term in (42) arises from the presence of the $\hat{p}$ normalization in the denominator of (37); the second, more important term translates precipitation error to runoff error. A crude estimate of the magnitude of the runoff sensitivity dy/dp will suffice; we use the semiempirical water-balance theory of Budyko (1974), applied to our estimates of the annual means, which yields a relation of the form (MIDUb; MIWE)

$$\frac{dy}{dp} = \Phi(\hat{y}/\hat{p}). \tag{43}$$

Because ε is a random variable, so is δ^*. We introduce Δ^* as a characteristic value of δ^* defined by

$$(\Delta^*)^2 = E\{(\delta^*)^2\}. \tag{44}$$

Squaring (42) and taking an expectation, using (43), we obtain

$$(\Delta^*)^2 = [\hat{\delta} - \Phi(\hat{y}/\hat{p})]^2 E\{\varepsilon^2\}/\hat{p}_a^2. \tag{45}$$

In conjunction with the estimates of the precipitation error $E\{\varepsilon^2\}$ from MIDUa through (36), (45) allows us to estimate the characteristic magnitude of the contribution of errors in precipitation to differences between modeled and observed runoff ratio. Ordinarily, Φ will dominate $\hat{\delta}$ in (45). The value of Φ ranges from 0 in a very arid climate to 1 in a very wet climate. Thus, the degree to which precipitation errors contaminate our comparisons of modeled and observed runoff ratios increases from a very small effect in arid climates to a maximum effect in wet climates.

d. Application and tuning of the model: NEW and TUNED results

The untuned performance of the model is illustrated in Fig. 4. A large amount of scatter is evident. However, much of the scatter is associated with data having relatively large precipitation uncertainty. Most of the data points with relatively small uncertainty scatter along a

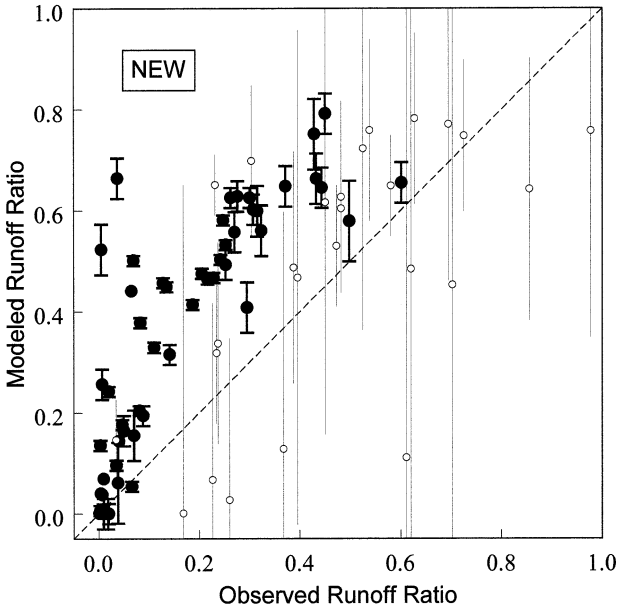

FIG. 4. Scatterplot of modeled runoff ratio against observed runoff ratio for the NEW experiment. Error bars denote ±1 characteristic error (Δ*) in runoff ratio resulting from error of precipitation. For clarity, basins with Δ* smaller than 0.1 are plotted with filled symbols and heavy error bars.

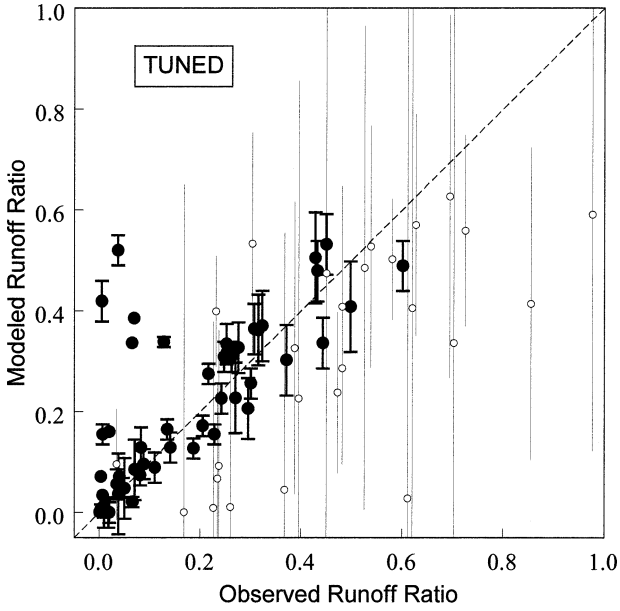

FIG. 5. Scatterplot of modeled runoff ratio against observed runoff ratio for the TUNED experiment (i.e., with all values of non-water-stressed bulk stomatal resistance reduced by a factor of 0.4). Error bars denote ±1 characteristic error (Δ*) in runoff ratio resulting from error of precipitation. For clarity, basins with Δ* smaller than 0.1 are plotted with filled symbols and heavy error bars.

line that rises from the origin with a slope of about 2, indicating excessive runoff by a factor of 2. Clearly, the NEW model run has a positive runoff bias.

The runoff bias appears too large to be explained by any systematic bias in the radiation forcing data, and precipitation uncertainty has already been incorporated into the analysis. The runoff error is clearly attributable to the model itself. On the basis of sensitivity analyses and assessment of the uncertainties in our values for the various parameters, we concluded that our estimates of the non-water-stressed bulk stomatal resistance were the most likely single cause of the runoff bias. Accordingly, we adjusted all values of this parameter by a single, globally constant scale factor. A value of 0.4 was found to bring the majority of the small-uncertainty points into the neighborhood of the 1-1 line (Fig. 5). In view of the precipitation errors, most of the points far from the 1-1 line are not clear indicators of model error. However, strong significance can be attached to positive runoff biases in a small number of basins observed with low runoff ratios; these will be discussed in the next subsection.

In retrospect, the need to reduce the assigned values of non-water-stressed bulk stomatal resistance is not surprising. The LaD model ignores the possibility of evaporation from interception and (except for desert) direct evaporation from soil, requiring all vapor to be transported through the ''big leaf'' of the model. In reality, the stomatal resistance is bypassed when vegetation is wetted externally by precipitation. Because evaporation from the interception store can be a substantial fraction of precipitation (Ward 1975), its neglect can contribute to a potentially significant negative bias in evaporation (and, hence, positive bias in runoff). By assigning a smaller value to the stomatal resistance parameter, we are crudely compensating for this model bias.

e. Analysis of outliers

A few basins in the TUNED run still have a major positive runoff bias that cannot be explained by precipitation errors (Fig. 5). They include the Niger, Benue, and Senegal River Basins in the Sahel region of Africa, the Sao Francisco River Basin in the Brazilian highlands, and the Blackwood River Basin in extreme southwestern Australia. We examined monthly time series of modeled water-balance components for these basins and found a common set of characteristics. All of these basins are in a region where climatic aridity is strongly seasonal. The annual-mean net radiation is much more than sufficient to evaporate the annual precipitation, but this climatic aridity is reversed during a brief wet season, when most of the precipitation falls. The observed mean hydrologic response is one of an arid region: only a small fraction of precipitation runs off. The model, however, can store an amount of water no greater than W_R^*, which is much less than the wet season excess of precipitation over evaporative potential of net radiation. Indeed, sensitivity analyses showed that the large runoff error in these basins would essentially disappear if the storage capacity were artificially quadrupled.

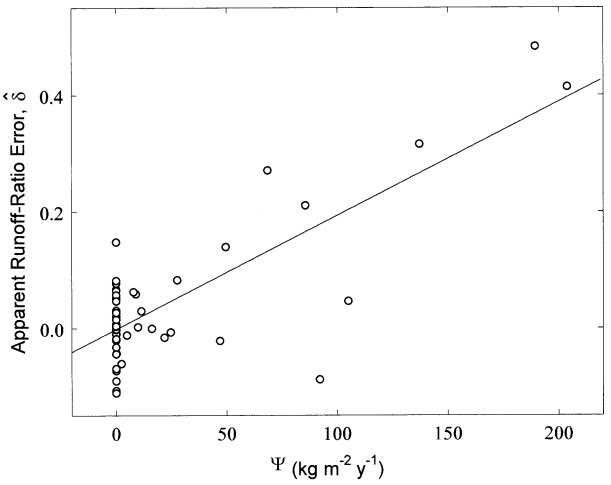

FIG. 6. Scatterplot of the apparent error in runoff ratio of the TUNED experiment against the climatic index Ψ. To clarify the analysis, data are plotted only for basins having Δ^* smaller than 0.1. Plotted line ($\hat{\delta} = -0.0017 + 0.0020\Psi$; $r = 0.78$) is the fitted least squares linear relation, whose slope is highly significant ($p < 10^{-6}$).

The interaction of two factors appears to explain the large runoff bias in some arid basins. The first is strong aridity in the annual mean; the second is a large excess of precipitation during a limited part of the year. Let $\overline{P}$ be the average annual precipitation and let $\overline{R_n}$ be the corresponding net radiation; one measure of annual aridity is the amount by which the index of dryness exceeds 1, $\overline{R_n}/L\overline{P} - 1$. A measure of the tendency of seasonal water excess to exceed the root zone storage capacity is $\int_{\text{year}} \max(P - R_n/L, 0)\, dt - W_R^*$. To quantify the interaction of these two factors, we introduced an index Ψ,

$$\Psi = \max[(\overline{R_n}/L\overline{P} - 1), 0] \times \max\left\{\left[\int_{\text{year}} \max(P - R_n/L, 0)\, dt - W_R^*\right], 0\right\}, \quad (46)$$

which we found to be a reasonably powerful indicator of the strong positive runoff biases remaining in the TUNED model run (Fig. 6). Note that this index is zero for most basins in the dataset. For Ψ to be nonzero, the basin must have an arid climate (the first factor), a wet season (period when P is greater than R_n/L) must exist, and the wet season excess water must be greater than the capacity of the soil to store the water for the dry season. The measure Ψ does incorrectly indicate that two or three additional basins should exhibit a large positive runoff bias, but this is a rather small ''false-positive'' failure rate, in view of the large number of basins correctly characterized.

Clearly, interseasonal water storage is underestimated for most basins with large Ψ in the TUNED model run. The true effective storage capacity of land may be greater than that in the model because of a greater effective rooting depth. An easy model adjustment would be to increase the rooting depth, at least in environments where Ψ is significantly large. In order to reconcile this with the data of Jackson et al. (1996), however, we would need either 1) to introduce biome-specific values of the critical root density at the bottom of the effective root zone or 2) to greatly increase the effective rooting depth globally. We prefer to avoid both of these alternatives; the first would reduce model parsimony considerably, and the second would require most model biomes to have root systems much deeper than they appear to need.

A soil-physical resolution of our quandary may exist. In the seasonally wet environments where the excessive runoff has been noted, we hypothesize that the wet season excess of precipitation first fills the root zone to field capacity, and subsequently brings the subroot soil to field capacity, essentially from the top downward; such behavior is what would be expected on the basis of standard soil physics. During the dry season, the root-zone soil water is depleted quickly by the intense aridity, and the resulting soil water gradient drives an upward diffusive flow into the root zone. Soil water transport is affected both by gravity and by nonlinear diffusion, but the present problem can be approximated by ignoring gravity and using an effective diffusion coefficient, D_θ. We idealize this as a problem of upward diffusion from a semi-infinite medium to a boundary at the bottom of the effective root zone. The subroot-zone depth of drying by upward diffusion will be on the order of $(4D_\theta\tau_D/\pi)^{1/2}$ (Hillel 1980, p. 125); here, τ_D is the duration of the dry season. For an order-of-magnitude analysis, we take typical values $D_\theta = 1000$ and 10 000 mm^2 d^{-1} (Hillel 1980, p. 143; Black et al., 1969; Eagleson 1978) and $\tau_D = 300$ d (length of dry season), obtaining effective drying depths of 600 and 2000 mm below the bottom of the root zone. These drying depths would require increases of the effective rooting depth (600 mm for the grass-lands where insufficient storage has been noted; Table 1) by substantial factors of 2–4. Such increases appear sufficient to eliminate most of the noted positive bias in modeled runoff. Implied directions for future model development are addressed in the summary and discussion.

f. Retrospective analysis: OLD, RS0, and RS0Z01 results

The purpose of the OLD experiment was to evaluate the performance of the Manabe (1969) model in the same framework as the new LaD model in order to assess whether the model ''improvements'' actually resulted in increased predictive power in a stand-alone mode. The OLD experiment results are shown in Fig. 7. The performance is good in many basins, but the model tends to underestimate the runoff ratio in some basins with intermediate values of the runoff ratio. Ad-

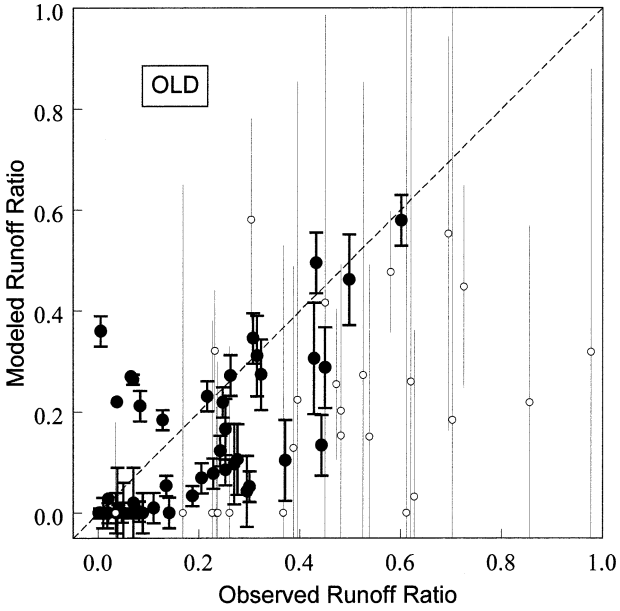

FIG. 7. Scatterplot of modeled runoff ratio against observed runoff ratio for the OLD experiment [i.e., with several reductions to the model to make it mimic the model of Manabe (1969)]. Error bars denote ±1 characteristic error (Δ*) in runoff ratio resulting from error of precipitation. For clarity, basins with Δ* smaller than 0.1 are plotted with filled symbols and heavy error bars.

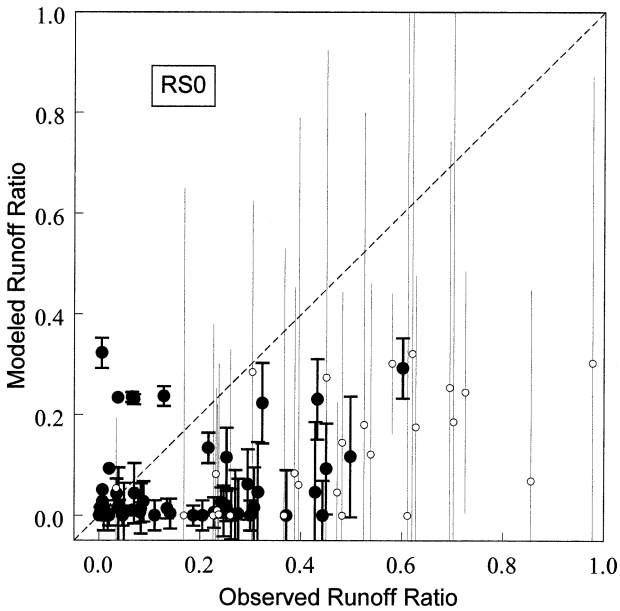

FIG. 8. Scatterplot of modeled runoff ratio against observed runoff ratio for the RS0 experiment (i.e., like NEW, but with $r_s = 0$). Error bars denote ±1 characteristic error (Δ*) in runoff ratio resulting from error of precipitation. For clarity, basins with Δ* smaller than 0.1 are plotted with filled symbols and heavy error bars.

ditionally, the scatter of points with low precipitation error in regions of intermediate wetness (observed runoff ratios of around 0.2–0.3) is significantly greater in OLD than in TUNED. In common with other experiments, OLD seriously overestimates runoff in some seasonally arid (large-Ψ) basins.

Given the fundamental differences between the TUNED and OLD experiments, the results of the OLD experiment are remarkably good. This issue deserves further analysis, as it suggests that solutions may be very insensitive to major changes in the model formulation. However, the model sensitivity to r_s is confirmed in Fig. 8, and can also be seen by comparison of Fig. 4 and Fig. 5. Elimination of stomatal resistance from the TUNED experiment causes so much evaporation that very little runoff occurs. Evidently, some one or more other differences between the TUNED and OLD experiments compensate partially for this great sensitivity to r_s. In fact, we found that the other main factor is the surface roughness length. By setting r_s to zero and both z_o and z_T to 0.01 m (the RS0Z01 experiment, Fig. 9) in what was otherwise identical to the TUNED experiment, we obtained results very similar to those in the OLD experiment. We conclude that these are the two most significant changes in the model, and that their mutual compensation was a factor hiding their individual errors in the original model.

The compensation can be understood qualitatively by appeal to an idealized solution of the surface flux equa-

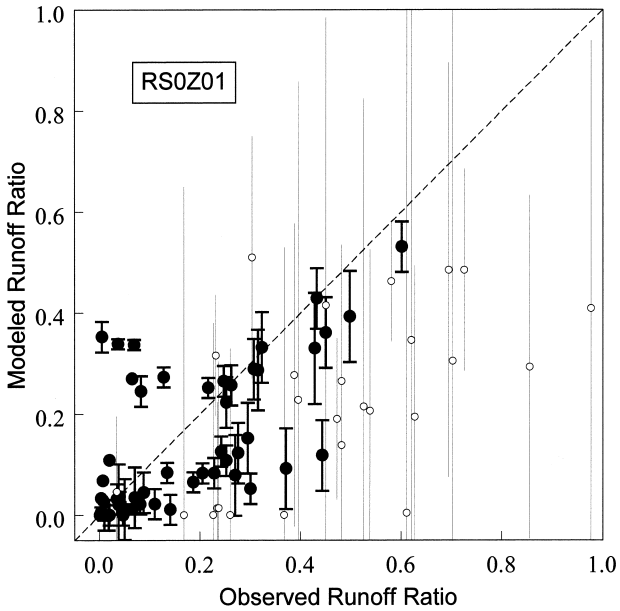

FIG. 9. Scatterplot of modeled runoff ratio against observed runoff ratio for the RS0Z01 experiment (i.e., like NEW, but with $r_s = 0$ and $z_o = z_T = 0.01$ m). Error bars denote ±1 characteristic error (Δ*) in runoff ratio resulting from error of precipitation. For clarity, basins with Δ* smaller than 0.1 are plotted with filled symbols and heavy error bars.

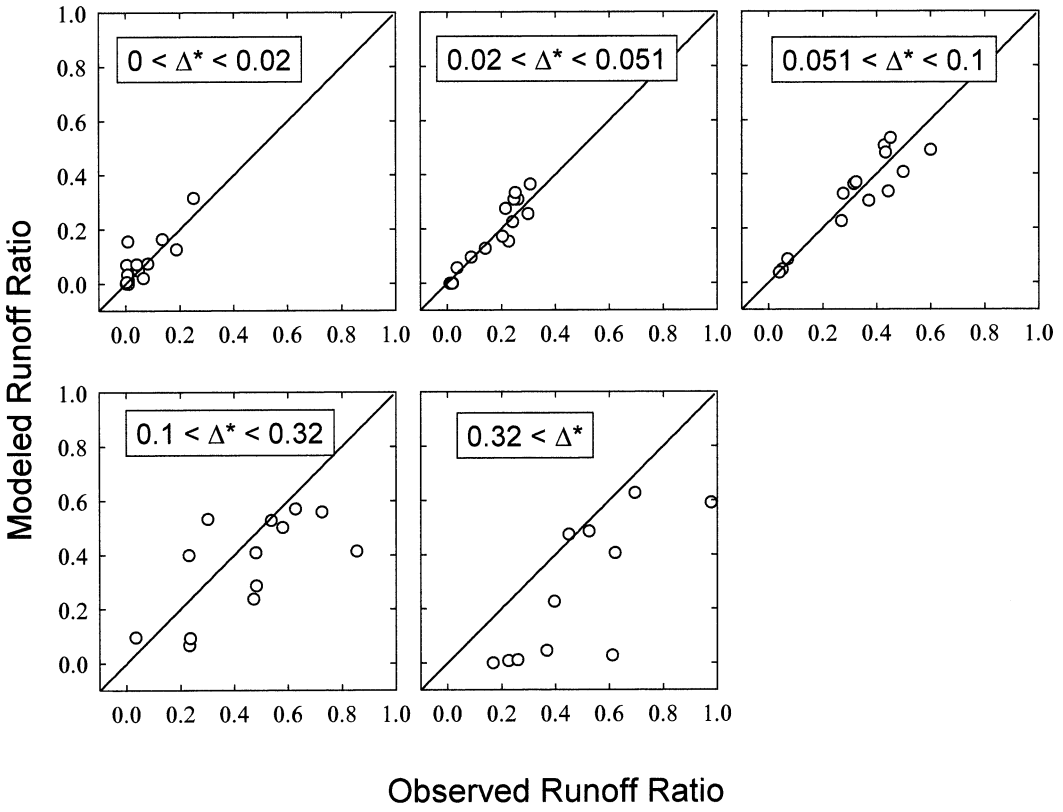

FIG. 10. Categorized scatterplots of modeled against observed runoff ratios for the TUNED experiment. Each panel is for a different range of Δ*, with the ranges chosen so that approximately equal numbers of points will fall in each panel. The vertical displacement of a point from the 1-1 line is the apparent runoff ratio error $\hat{\delta}$. Basins for which $\Psi > 40$ kg m^{-2} y^{-1} were excluded.

tions for a non-water-stressed surface (Brutsaert 1982, p. 224),

$$LE = \frac{sR_n + (\rho c_p V)/r_a}{s + \gamma(1 + r_s/r_a)}, \tag{47}$$

where s is the temperature derivative of saturation vapor pressure, γ is the psychrometric constant, and V is the near-surface vapor pressure deficit of the air. Generally, s and γ are of the same order of magnitude, as are r_s and r_a. Setting r_s to zero in (47) causes significant overestimation of E, which translates to an opposite error in runoff. But if r_a also is increased to a large value (by decreasing the surface roughness length greatly), then the V term in (47) can be reduced greatly, compensating for the first error.

g. *Consistency between model results and precipitation error estimates*

We have already seen that the greatest apparent runoff ratio errors in the TUNED experiment generally are associated with the larger values of Δ*, as expected. Here we examine more closely the relation between the apparent runoff ratio errors $\hat{\delta}$ and their expected component caused by precipitation error, Δ*. Figure 10, which excludes those few basins for which Ψ is large, shows that the scatter away from the 1-1 line is smallest in the two panels with Δ* less than 0.051, somewhat larger for Δ* up to 0.1, and even larger for larger values of Δ*.

To quantify this apparent growth in dispersion of $\hat{\delta}$ with that of Δ*, we bin the observations into 10 ranges of Δ* values and calculate root-mean-square values, denoted by RMS(Δ*) and RMS($\hat{\delta}$), over the subsets of data within each range. A scatterplot of RMS($\hat{\delta}$) against RMS(Δ*) is shown in Fig. 11. From (38), we can predict the form of the relation between RMS($\hat{\delta}$) and RMS(Δ*). Under the reasonable assumption that intrinsic model error is independent of precipitation estimation error, we find

$$E\{(\hat{\delta})^2\} = E\{\delta^2\} + E\{(\delta^*)^2\}, \tag{48}$$

or, equivalently,

$$\mathrm{RMS}(\hat{\delta}) = [\Delta^2 + [\mathrm{RMS}(\Delta^*)]^2]^{1/2}, \tag{49}$$

where the intrinsic model error is characterized by

$$\Delta^2 = E\{\delta^2\}. \tag{50}$$

The TUNED model results follow this relation (Fig. 11). When precipitation error is large, the apparent model

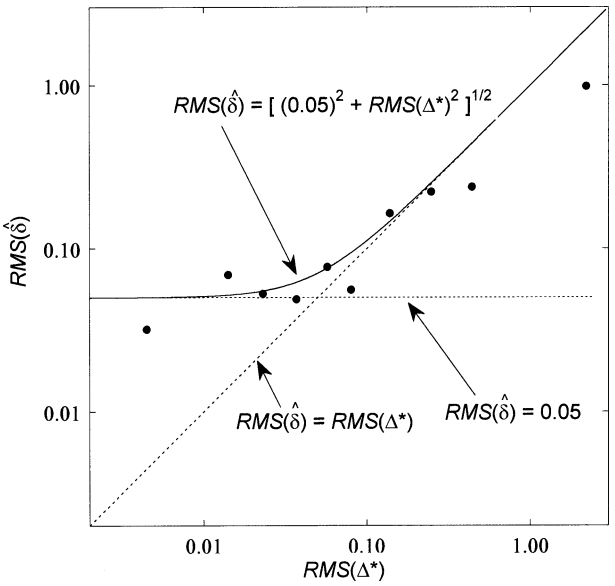

FIG. 11. Scatterplot of root-mean-square values of apparent runoff ratio error against root-mean-square values of Δ^*, the characteristic runoff ratio error expected to result from precipitation error. Each point represents six or seven basins. Basins for which $\Psi > 40$ kg m^{-2} y^{-1} were excluded. Curved line is the least squares fit of the expression (49).

error is dominated by the precipitation error. When precipitation error is small, the apparent model error is equal to the intrinsic model error. A least squares fit (based on relative differences) of the data implies that the intrinsic model error in the TUNED run (with exclusion of identified outliers) is 0.05, meaning that the model runoff typically would deviate from the observed runoff by 5% of precipitation in the absence of precipitation errors. The fit of the data to the theoretical expression (49) is evidence of the validity of MIDUa's precipitation error estimates and of their realistic conversion to induced runoff errors through (45).

4. Summary and discussion

a. New model

We have described and tested, in stand-alone mode, a new model of land water and energy balance. The Land Dynamics (LaD) model is an outgrowth of the model of Manabe (1969), incorporating the following new features:

- non-water-stressed stomatal control of transpiration, in order to correct a tendency toward excessive evaporation;
- vegetation and soil dependence of all surface parameters, in order to provide more realistic representation of geographic variations in water and energy balances and to enable model-based investigations of land-cover change;
- soil sensible heat storage and transport, in order to lay the groundwork for more realistic diurnal-cycle modeling in the future;
- a groundwater (saturated-zone) storage reservoir, in order to provide more realistic temporal variability of runoff; and
- a rudimentary runoff-routing scheme for delivery of runoff to the ocean, in order to provide realistic freshwater forcing of the ocean general circulation model component of a global climate model.

b. Model evaluation with uncertain precipitation

The performance of the new model has been evaluated in stand-alone mode with observational data on forcing and runoff ratios of major river basins of the world. Special attention was given to distinguishing between two components of the apparent runoff ratio error: the part due to intrinsic model error and the part due to errors in the assumed precipitation forcing. This decomposition proved extremely valuable in assessing the significance of discrepancies between modeled and observed runoff. Furthermore, the credibility of the precipitation error methods and estimates of MIDUa were strengthened by their consistency with the distribution of differences between observed and modeled runoff ratios. Our various analyses support the contention that quantitative assessment of precipitation errors should be an integral part of any observation-based evaluation of land models.

Oki et al. (1999) hypothesized that the contribution of precipitation errors to apparent relative errors in modeled runoff could be quantified by rain gauge density. They concluded that apparent error was insensitive to density (and, presumably, negligible) when density exceeded 30–50 gauges per million square kilometers. Our findings differ considerably from these. Our estimates of δ_i^*, which predicted runoff errors well, were only very weakly correlated with gauge density, which was not a good predictor of runoff error. Of the 82 basins used for the analysis, only one had a density lower than 30 gauges per million square kilometers, although many were judged inadequately gauged for model evaluation.

c. Soil-moisture diffusion or deep roots as mechanisms of interseasonal water storage

Our error-based model-performance analysis provided strong evidence for a positive runoff bias in typically subtropical regions where a climate that is very arid in the mean has a brief, intense wet season. In the framework of the model, this bias can be removed only by increasing the depth of the root zone by a factor of about 4. On the other hand, it appears that the error may be explained by our neglect of upward soil water diffusion from below the root zone during the dry season. In our model, as in many such models, free gravity drainage is assumed at the bottom of the root zone, meaning that

water cannot flow upward across this plane. The effect of soil water diffusion on a seasonal timescale could be incorporated artificially by a theoretically derived, climate-dependent increase of the effective rooting depth based on an analysis of the type outlined herein. Alternatively, the process could be represented explicitly with a one-dimensional diffusion equation. Many land models already include such an equation, although it is not clear that sufficient attention has been given to its accurate formulation and solution for this application. In addition to the commonplace prescription of gravity drainage at the bottom of the root zone, nearly all models have far fewer layers than necessary for accurate numerical solutions (Milly and Eagleson 1982; Milly 1984).

Nepstad et al. (1994) noted that rooting depths commonly assumed in climate models appeared insufficient to explain the observed amount of dry season evapotranspiration at field sites in Brazilian Amazonia. They inferred that deep roots, characterized by relatively low biomass density, were responsible for substantial water uptake from depths of 2–8 m and greater. Subsequently, some modelers have applied this idea. Zeng et al. (1998) considered defining the root-zone depth as the depth where root density decayed to 1% of its surface value. (This approach is different from ours, which is based on the actual density itself.) Because the 1% value of rooting depth was judged to be too small, they considered the use of maximum observed rooting depths, but these were rejected for being too large. Thus, they settled on the geometric mean of the 1% value and the maximum observed value. Neither of these values seems very directly related to the ability of plants to withdraw water, and the latter value is perhaps as much determined by the history of measurements as it is by intrinsic plant properties. Kleidon and Heimann (1998) applied the hypothesis (Milly and Dunne 1994; Milly 1994) that ecosystems will have rooting depths large enough to maximize evapotranspiration. As applied, however, their method extracted no cost for growth of roots, and, therefore, their rooting depths may have been unrealistically large. Furthermore, their use of a ''bucket'' soil water reservoir, similar to that used in this study, could have artificially forced the plants to extend their roots, given the model-enforced absence of upward soil water diffusion. In view of our analysis, it appears that inferences of water uptake by deep roots may have been biased in these various studies by the neglect of soil water diffusion.

d. Stomatal resistance, interception loss, and evaporation from soil

The model was crudely tuned by varying a globally constant scale factor on non-water-stressed bulk stomatal resistance. In order to match observed basin runoff, it was necessary to reduce the global field of this resistance by a factor of 0.4. The size of this adjustment is substantial. Part of the adjustment might be attributed to the crudeness by which we averaged the values of Dorman and Sellers (1989) subjectively over the seasonal cycle and adjusted subjectively for stresses not included in their analysis. It also could be argued that some allowance must be made for the enormous difference in scale between fundamental biophysical measurements and model application. However, we do not expect these issues to lead to a global bias large enough to explain the factor of 0.4. We believe that our neglect of interception loss (in humid environments) and direct evaporation from soil (in semiarid environments) may be at least as important as these other factors for explaining the noted discrepancy.

e. Retrospective analysis of predecessor model

The new model was shown to perform better than the predecessor model of Manabe (1969), which itself performed in a fair manner. The performance of the old model appears to be explained by mutual compensation of two substantial biases: those due to neglect of stomatal resistance and due to specification of unrealistically small surface roughness lengths. Overall, the former bias dominates, leading to generally excessive evaporation in stand-alone experiments.

Comparison of various numerical experiments suggests that most of the quantitative difference in annual runoff between the old and new models is associated with the two factors just mentioned. This suggests that other model changes have relatively little effect on the annual water and energy balance. This result is to be expected for the groundwater storage and surface water routing features, which do not feed back to the water balance. More interesting is the implied insensitivity of the model to the introduction of soil- and vegetation-dependent land parameters. In Parts II (Milly and Shmakin 2002) and III (Shmakin et al. 2002) of this series of papers, we attempt to determine whether estimates of global variations in land parameters contribute in a measurable way to model performance. Part II examines geographic variations in runoff ratio for an individual year, while Part III addresses geographic variations of runoff sensitivity to interannual variability of climate.

f. Focus on annual timescale

The focus of this analysis has been on annual-mean runoff as an indicator of long-term water and energy balances. It must be acknowledged that the ability to reproduce long-term balances does not imply equivalent ability to model short-term response. It is, however, a necessary condition. We believe that model development should be an evolutionary process, guided by the feedback obtained from ongoing comparisons with observations and accompanying diagnostic and theoretical analyses. An initial focus on the annual timescale may be an efficient strategy in the long run.

Acknowledgments. This work was facilitated by ongoing modeling-system developments at GFDL; in particular, we wish to acknowledge contributions by Jeff Anderson, Isaac Held, Steve Klein, and Bruce Wyman. Financial support for A.B.S. was provided by NASA's Water Cycle Processes Program through the University Corporation for Atmospheric Research. Helpful reviews were provided by Isaac Held and Guiling Wang.

REFERENCES

Black, T. A., W. R. Gardner, and G. W. Thurtell, 1969: The prediction of evaporation, drainage and soil water storage for a bare soil. *Soil Sci. Soc. Amer. Proc.,* **33,** 665–660.

Brutsaert, W. H., 1982: *Evaporation into the Atmosphere: Theory, History, and Applications.* D. Reidel, 299 pp.

Budyko, M. I., 1974: *Climate and Life.* Academic, 508 pp.

Chen, T. H., and Coauthors, 1997: Cabauw experimental results from the Project for Intercomparison of Land–Surface Parameterization Schemes. *J. Climate,* **10,** 1194–1215.

Costa, M. H., and J. A. Foley, 1997: Water balance of the Amazon basin: Dependence on vegetation cover and canopy conductance. *J. Geophys. Res.,* **102D,** 23 973–23 989.

Delworth, T. L., and S. Manabe, 1989: The influence of soil wetness on near-surface atmospheric variability. *J. Climate,* **2,** 1447–1462.

Dickinson, R. E., J. Jaeger, W. M. Washington, and R. Wolski, 1981: Boundary subroutine for the NCAR global climate model. National Center for Atmospheric Research Tech. Note TN-173+1A, 75 pp.

Dorman, J. L., and P. J. Sellers, 1989: A global climatology of albedo, roughness length and stomatal resistance for atmospheric general circulation models as represented by the Simple Biosphere Model (SiB). *J. Appl. Meteor.,* **28,** 833–855.

Dunne, K. A., and C. J. Willmott, 1996: Global distribution of plant-extractable water capacity of soil. *Int. J. Climatol.,* **16,** 841–859.

Eagleson, P. S., 1978: Climate, soil, and vegetation. 3. A simplified model of soil moisture movement in the liquid phase. *Water Resour. Res.,* **14,** 722–730.

Garratt, J. R., 1992: *The Atmospheric Boundary Layer.* Cambridge University Press, 316 pp.

Haywood, J. M., R. J. Stouffer, R. T. Wetherald, S. Manabe, and V. Ramaswamy, 1997: Transient response of a coupled model to estimated changes in greenhouse gas and sulfate concentrations. *Geophys. Res. Lett.,* **24,** 1335–1338.

Henderson-Sellers, A., Z.-L. Yang, and R. E. Dickinson, 1993: The Project for Intercomparison of Land-Surface Parameterization Schemes. *Bull. Amer. Meteor. Soc.,* **74,** 1335–1349.

——, K. McGuffie, and C. Cross, 1995: Sensitivity of global climate model simulations to increased stomatal resistance and CO_2 increases. *J. Climate,* **8,** 1738–1756.

Hillel, D., 1980: *Applications of Soil Physics.* Academic, 385 pp.

Jackson, R. B., J. Canadell, J. R. Ehleringer, H. A. Mooney, O. E. Sala, and E. D. Schulze, 1996: A global analysis of root distributions for terrestrial biomes. *Oecologia,* **108,** 389–411.

Kleidon, A., and M. Heimann, 1998: Optimised rooting depth and its impact on the simulated climate of an Atmospheric General Circulation Model. *Geophys. Res. Lett.,* **25,** 345–348.

Koster, R. D., and M. J. Suarez, 1996: Energy and water balance calculations in the Mosaic LSM. NASA Tech. Memo. 104606, 60 pp.

Levis, S., M. T. Coe, and J. A. Foley, 1996: Hydrologic budget of a land surface model: A global application. *J. Geophys. Res.,* **101D,** 16 921–16 930.

Lohmann, D., R. Nolte-Holube, and E. Raschke, 1996: A large-scale horizontal routing model to be coupled to land surface parameterization schemes. *Tellus,* **48A,** 708–721.

——, and Coauthors, 1998: The Project for Intercomparison of Land-Surface Parameterization Schemes (PILPS) phase 2(c) Red–Arkansas River basin experiment. 3. Spatial and temporal analysis of water fluxes. *Global Planet. Change,* **19,** 161–179.

Manabe, S., 1969: Climate and the ocean circulation. 1. The atmospheric circulation and the hydrology of the earth's surface. *Mon. Wea. Rev.,* **97,** 739–774.

Matthews, E., 1983: Global vegetation and land use: New high-resolution data bases for climate studies. *J. Climate Appl. Meteor.,* **22,** 474–487.

Meeson, B. W., F. E. Coprew, J. M. P. McManus, D. M. Myers, J. W. Closs, K.-J. Sun, D. J. Sunday, and P. J. Sellers, 1995: *ISLSCP Initiative I—Global Data Sets for Land–Atmosphere Models, 1987–1988,* Vols. 1–5, NASA, CD-ROM, USA_NASA_GDAAC_ISLSCP_001/002/003/004/005.

Milly, P. C. D., 1984: A simulation analysis of thermal effects on evaporation from soil. *Water Resour. Res.,* **20,** 1087–1098.

——, 1992: Potential evaporation and soil moisture in general circulation models. *J. Climate,* **5,** 209–226.

——, 1994: Climate, soil water storage, and the average annual water balance. *Water Resour. Res.,* **30,** 2143–2156.

——, and P. S. Eagleson, 1982: Parameterization of moisture and heat fluxes across the land surface for use in atmospheric general circulation models. R. M. Parsons Laboratory Tech. Rep. 279, Massachusetts Institute of Technology, 226 pp.

——, and K. A. Dunne, 1994: Sensitivity of the global water cycle to the water-holding capacity of land. *J. Climate,* **7,** 506–526.

——, and A. B. Shmakin, 2002: Global modeling of land water and energy balances. Part II: Land-characteristic contributions to spatial variability. *J. Hydrometeor.,* 296–307.

Nepstad, D. C., and Coauthors, 1994: The role of deep roots in the hydrological and carbon cycles of Amazonian forests and pastures. *Nature,* **372,** 666–669.

Oki, T., and Y. C. Sud, 1998: Design of Total Runoff Integrating Pathways (TRIP)—A global river channel network. *Earth Interactions,* **2.** [Available online at http://EarthInteractions.org.]

——, T. Nishimura, and P. Dirmeyer, 1999: Assessment of annual runoff from land surface models using Total Runoff Integrating Pathways (TRIP). *J. Meteor. Soc. Japan,* **77,** 235–255.

Schlosser, C. A., and Coauthors, 2000: Simulations of a boreal grassland hydrology at Valdai, Russia: PILPS phase 2(d). *Mon. Wea. Rev.,* **128,** 301–321.

Sellers, P. J., Y. Mintz, Y. C. Sud, and A. Dalcher, 1986: A Simple Biosphere Model (SiB) for use within atmospheric general circulation models. *J. Atmos. Sci.,* **43,** 505–531.

——, and Coauthors, 1996a: Comparison of radiative and physiological effects of doubled atmospheric CO_2 on climate. *Science,* **271,** 1402–1406.

——, and Coauthors, 1996b: A revised land surface parameterization (SiB2) for atmospheric GCMs. Part I: Model formulation. *J. Climate,* **9,** 676–705.

Shmakin, A. B., P. C. D. Milly, and K. A. Dunne, 2002: Global modeling of land water and energy balances: Part III: Interannual variability. *J. Hydrometeor.,* 308–323.

Times Books, 1988: *The Times Atlas of the World.* 7th ed. Times Books Limited, 228 pp. and 123 plates.

U.S. National Research Council, 1990: *Research Strategies for the U.S. Global Change Research Program.* National Academy Press, 291 pp.

——, 1998: *GCIP, Global Energy and Water Cycle Experiment (GEWEX) Continental-Scale International Project: A Review of Progress and Opportunities.* National Academy Press, 93 pp.

Ward, R. C., 1975: *Principles of Hydrology.* 2d ed. McGraw-Hill, 367 pp.

Zeng, X., Y.-J. Dai, R. E. Dickinson, and M. Shaikh, 1998: The role of root distribution for climate simulation over land. *Geophys. Res. Lett.,* **25,** 4533–4536.

Zhang, C., D. A. Dazlich, and D. A. Randall, 1999: Simulations of soil moisture and surface water balance using the Simple Biosphere Model 2. *J. Meteor. Soc. Japan,* **77,** 217–234.

Zobler, L. 1986: A world soil file for global climate modeling. National Aeronautics and Space Administration Tech. Memo. 87802, 33 pp.